Electronic structure changes of Si(001)-(2×1) from subsurface Mn observed by STM

M. R. Krause, A. J. Stollenwerk, J. Reed, and V. P. LaBella*
The College of Nanoscale Science and Engineering, The University at Albany-SUNY, Albany, New York 12203, USA

M. Hortamani, P. Kratzer,† and M. Scheffler
Fritz-Haber-Institut der Max-Planck-Gesellschaft, Faradayweg 4-6, D-14195 Berlin-Dahlem, Germany
(Received 13 October 2006; revised manuscript received 8 March 2007; published 18 May 2007)

The deposition of Mn atoms onto the Si(001)-(2×1) reconstructed surface has been studied using scanning tunneling microscopy (STM) and first-principles electronic structure calculations. Room-temperature deposition of 0.1 ML (monolayer) of Mn gives rise to a disordered surface structure. After *in situ* annealing between 300 and 700 °C, most of the Mn is incorporated into three-dimensional manganese silicide islands, and Si dimer rows reappear in the STM images on most of the substrate surface. At the same time, rowlike structures are visible in the atomic-scale STM images. A comparison with calculated STM images provides evidence that Mn atoms are incorporated into the row structures in subsurface interstitial sites, which are the lowest-energy position for Mn on Si(001). The subsurface Mn alters the height and local density of states of the Si dimer atoms, causing them to appear 0.6 Å higher than a neighboring Si dimer with no Mn below. This height difference that allows the detection the subsurface Mn results from a subtle interplay of geometrical and electronic effects.

DOI: 10.1103/PhysRevB.75.205326 PACS number(s): 68.47.Fg, 68.37.Ef, 68.55.Ac

I. INTRODUCTION

In recent years, several aspects of the interaction of manganese atoms with silicon surfaces have attracted attention. It has been speculated that incorporation of Mn on substitutional sites of the Si lattice using nonequilibrium growth techniques could turn silicon into a dilute magnetic semiconductor,[1,2] similar to Mn incorporation in Ge,[3,4] or could be used to achieve δ doping of Si with possible applications as spin valves.[3,5] An alternative route to spintronics applications focuses on heterostructures formed by magnetic metal layers on silicon. Such heterostructures could be used as Schottky diodes for injection of a spin-polarized current, a concept that has been successfully demonstrated already for nonmagnetic tunnel contacts.[6] Theoretical considerations suggest that epitaxial MnSi thin films should order ferromagnetically on Si(001).[7] This has lead to the expectation that MnSi films on Si could be used to fabricate magnetic heterostructures by molecular-beam epitaxy.

A number of studies have been devoted to the growth of manganese silicides on silicon (see Ref. 8 and references therein). It has been found that ultrathin films on Si(001) tend to form three-dimensional manganese silicide clusters upon annealing,[9] and these clusters undergo a ripening process at annealing temperatures of 300–700 °C.[8] No closed and flat films of Mn or MnSi on Si(001) have been reported to date. However, the ripening process that takes place during annealing involves material exchange between the clusters. If the sample is quenched to room temperature, a finite concentration of mobile Mn adatoms present between the three-dimensional islands can be retained. Recent calculations by some of the present authors using density-functional theory (DFT) predict that the lowest-energy position for Mn atoms on the Si(001) surface is a subsurface interstitial site.[7,10] However, images that show the effect of these interstitial Mn atoms have not been presented.

In this paper, the Si(100) surface is imaged with scanning tunneling microscopy (STM) after deposition of a small amount of Mn atoms and subsequent annealing, and rowlike structures on the Si(001)-(2×1) reconstructed surface with a local $c(4\times2)$ periodicity are found. By comparing the experimental images with DFT calculations, these structures are identified as $c(4\times2)$-periodic arrangements of Mn atoms occupying subsurface interstitial sites.

II. EXPERIMENT

The experiments were carried out in a combined molecular-beam epitaxy and scanning tunneling microscopy (STM) multichamber ultrahigh-vacuum (UHV) facility.[11] Commercially available Si(001) wafers [B doped, $(1.75\pm0.75)\times10^{-3}$ Ω cm] were diced into 10×2 mm^2 rectangular pieces and cleaned *ex situ* in an ultrasonic acetone bath. They were clamped in sample holders made of Ta, which had been previously cleaned by heating a sacrificial silicon sample at approximately 1250 °C for a period of 24 h under UHV conditions. The samples were introduced into UHV through a load lock. A conventional *in situ* preparation process of annealing and flashing the sample was used in order to create a clean, flat Si(001)-(2×1) reconstructed surface, which was confirmed by *in situ* STM imaging.[11] The sample was annealed using direct current heating, and the temperature was measured using an infrared pyrometer.

One-tenth of a monolayer of Mn was deposited using an electron-beam evaporator while the substrate was at room temperature (23 °C). The deposition rate was measured using a quartz microbalance, and the chamber pressure was below 5×10^{-10} mbar during the deposition. To observe the effect of annealing, some samples were annealed at 650 °C for 15 min and then cooled to room temperature and transferred under UHV conditions to the STM, while other samples were transferred to the STM without any postdeposition annealing. The STM images were acquired at room temperature with a constant tunneling current of about

0.1 nA and a tip bias of about 2.5 V. These tunneling parameters were found to give the best image quality, and systematic bias dependent imaging was not performed. The base pressure in the STM chamber was below 3×10^{-11} mbar.

III. CALCULATIONS

For comparison with the STM measurements, we performed DFT calculations of atomic configurations that are likely to occur during the initial stages of growth. A comprehensive summary of all the structures considered is published elsewhere.[10] The adsorption of Mn atoms on Si(001) is described using a slab model of the surface. DFT total-energy calculations are performed using the PBE functional for electronic exchange and correlation and the (L)APW +lo approach to electronic structure calculations, as implemented in the WIEN2k computer code.[12] The uppermost three Si layers of the slab were fully relaxed until the forces on each moveable atom were smaller than 0.05 eV/Å. STM images were simulated within the Tersoff-Hamann approximation[13] by integrating the electronic density of states in an energy interval between the Fermi energy ϵ_F and ϵ_F-1 eV, which corresponds to filled-state images.

We took the energy interval of states contributing to the tunneling current narrower than expected from the overall experimental voltage drop between tip and sample, assuming that part of the applied voltage drops in the sample (e.g., due to band bending), rather than between the tip and the sample surface. Subsequently, the height above the surface for an isocontour surface of 10^{-5} eV/bohr^3 was calculated and plotted. Using a smaller energy window of 0.5 eV to define the density of states contributing to the tunneling current had little effect on the computed images. Likewise, empty-state images were computed by integrating the electronic density of states in an energy interval between the Fermi energy ϵ_F and ϵ_F+1 eV. However, these images were found to give little additional information and are not shown here.

IV. RESULTS

The STM images taken after deposition of 0.1 ML (monolayer) of Mn at room temperature onto the clean Si(001)-(2×1) reconstructed surface shows a rather unstructured surface with a random distribution of small clusters, as displayed in Fig. 1(a). In addition, this image displays a single height step of the underlying Si(001) surface running vertically up the image. The STM images taken from samples annealed after deposition at temperatures between 300–700 °C display the formation of three-dimensional islands, (not shown), while between the islands, the dimer rows of the Si(001)-(2×1) reconstruction become visible again as displayed in Figs. 1(b)–1(f).[8] In these images, the defect density in the flat areas between the islands is significantly higher than prior to the deposition. In addition to the defects, bright rowlike structures can be observed that run in the [110] direction, perpendicular to the underlying dimer rows of the Si(001)-(2×1) reconstruction. Two or more of these rows sometimes form adjacent to each other, resulting in two-dimensional structures with a local $c(4\times2)$ periodicity as highlighted by a rectangular box in Fig. 1(e). The bright rows are about 1.1 Å higher than the adjacent atoms as indicated by the height cross section shown in Fig. 1(g), which is taken from the dashed line in Fig. 1(f).

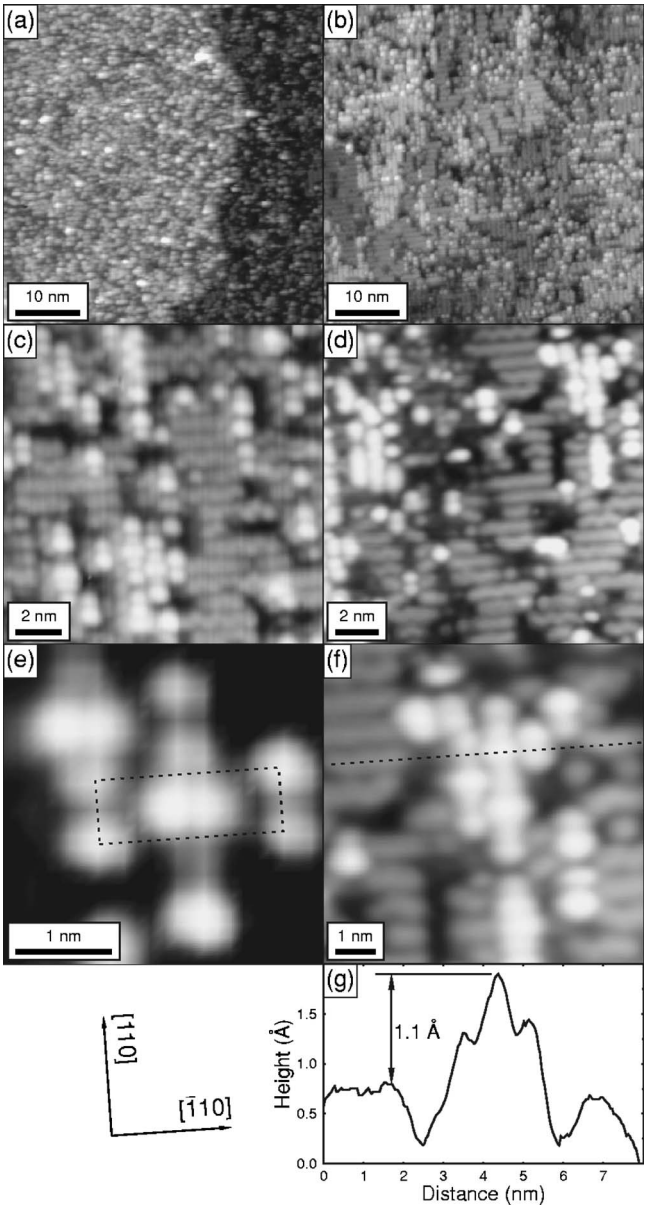

FIG. 1. STM images of (a) the Si(001)-(2×1) reconstructed surface after deposition of 0.1 ML of Mn at room temperature and [(b)–(f)] after deposition of 0.1 ML Mn at room temperature and subsequent annealing at 650 °C at different resolutions as indicated. The rows running in the $[1\bar{1}0]$ direction consist of Si dimers known from the clean substrate. The bright features running in the [110] direction include Mn atoms. (e) A contrast enhanced inset of (c) with a $c(4\times2)$ unit cell highlighted with the dashed box. (g) Height cross section taken from the region in image (f) as indicated by the dashed line.

Several computed STM images, using the Tersoff-Hamann approximation, are displayed in Figs. 2 and 3. The clean Si(001)-(2×2) reconstructed surface showing the buckled Si dimers running in the $[1\bar{1}0]$ direction is displayed

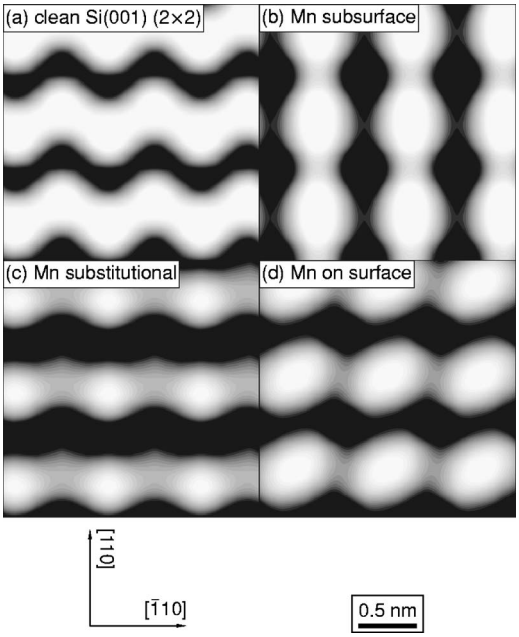

FIG. 2. Theoretically computed images using the Tersoff-Hamann approximation (surfaces of constant density of filled states down to 1 eV below the Fermi energy) for (a) clean Si(100), (b) Mn incorporated into subsurface interstitial site, (c) Mn in a substitutional site, and (d) Mn in a on-surface site.

in Fig. 2(a). Three images for (2×2) arrangements of Mn atoms in three different sites on the Si(001) surface, subsurface, substitutional, and on surface are displayed in Figs. 2(b)–2(d), respectively. The Mn subsurface location alters the surface of constant charge density by making the rows run in the [110] direction, perpendicular to the original dimer row direction, while the other two Mn locations do not alter the row direction. In the computed empty-state images, the zigzag rows characteristic of the clean Si(001)-(2×2) surface are inverted and show less corrugation, as has been observed earlier.[14] For Mn in the substitutional site, the Mn atom is less visible in the empty-state image than in the

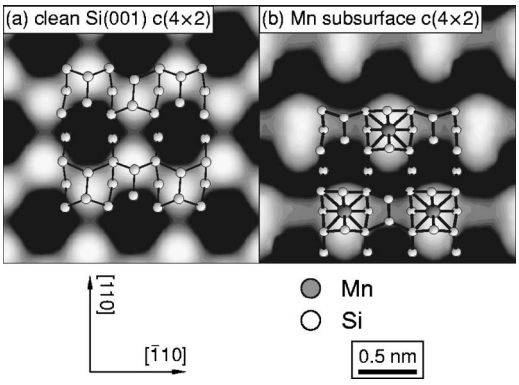

FIG. 3. Theoretically computed images using the Tersoff-Hamann approximation (surfaces of constant density of filled states down to 1 eV below the Fermi energy) for (a) clean Si(100) in the $c(4\times2)$ reconstruction and (b) Mn in a subsurface interstitial site in a $c(4\times2)$ reconstruction. Ball and stick models are also included for clarity.

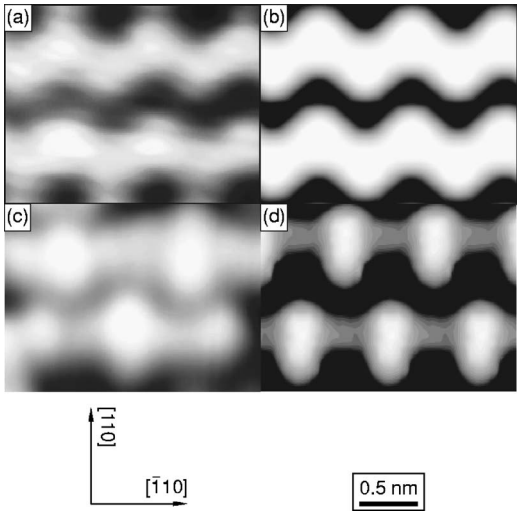

FIG. 4. Comparison of experimental images [left column, (a) and (c)] and theory [right column, (b) and (d)] for filled-state images of the clean Si(001) $c(4\times2)$ surface [upper row, (a) and (b)] and after Mn deposition [lower row, (c) and (d)]. While theory and experiment are in close agreement for the same surface structure, the two structures give clearly distinct images in both theory and experiment.

filled-state image. For both the on-surface and the subsurface position of Mn only, very little changes are observed between computed filled-state and empty-state images.

Comparison of computed images of $c(4\times2)$ reconstructed surfaces are displayed in Fig. 3. A calculated image of the clean Si(001)-$c(4\times2)$ reconstructed surface showing the buckled Si dimers running in the $[1\bar{1}0]$ direction is displayed in Fig. 3(a). In addition, the computed surface showing the effect of Mn incorporated into the subsurface site arranged in a $c(4\times2)$ periodicity is displayed in Fig. 3(b). The image with subsurface Mn is clearly different from the clean $c(4\times2)$ reconstruction with rows running in the same direction as the buckled dimers. While the bright features in the image of the clean surface in Fig. 3(a) occur at the positions of the lower Si atom of the Si dimers, the bright features in Fig. 3(b) are centered above the Si dimers with Mn atoms in the subsurface position below.

A comparison between the experimentally obtained STM images and DFT computed surfaces of constant density of states is displayed in Fig. 4. For reference, a high-resolution image of the clean Si(001)-(2×2) reconstructed surface taken at 77 K showing the buckled dimers along with the DFT computed image showing the same morphology is displayed in Figs. 4(a) and 4(b), respectively. A high-resolution STM image of one of the rowlike features observed after Mn deposition and annealing and the computed image of the $c(4\times2)$ arrangement of Mn in the subsurface position are displayed in Figs. 4(c) and 4(d), respectively. In these images, similar morphologies can be observed within the rows along with the out-of-phase arrangement between the adjacent rows.

A height cross section taken from the STM image shown in Fig. 1(f) across three of the rows observed after Mn deposition is plotted along with a similar height cross section

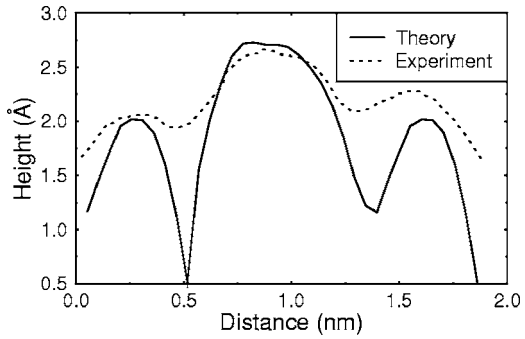

FIG. 5. Line scan perpendicular to the rows with local $c(4\times2)$ structure (dashed line) along the marked line in Fig. 1(f) and from the DFT calculations (solid line).

taken from the DFT image shown in $c(4\times2)$ and displayed in Fig. 5. Both plots show three peaks separated by the same distance with the center peak about 0.6 Å above the other two.

V. DISCUSSION

The surface morphology observed in Fig. 1(a) after Mn deposition onto the Si(100) surface is consistent with a Volmer-Weber (islanding) growth mode. This is in agreement with conclusions drawn from our DFT calculations,[7,10] which show that the formation of a very thin film of MnSi on Si(001) would be thermodynamically unfavorable. In addition, the formation of the larger MnSi islands after annealing is consistent with previous observations for Mn deposition and annealing on this surface.[8,9] The rowlike structures observed in the STM images between the islands displayed in Fig. 1 are not typically observed on clean Si(001) surfaces. Therefore, we conclude that these structures must arise from the Mn deposition and annealing. It has been previously determined that the large Mn-Si islands undergo an Ostwald ripening process,[8] which necessitates the exchange of material between islands, and thus these rowlike structures could possibly result from the freezing of these mobile Mn adatoms during the ripening process.

The STM images alone do not indicate the type of species that exist in the observed structures. However, much insight can be gained by comparing these images with both the theoretical STM images presented here and previous studies in the literature about defects or islands on the Si(001) surface. It is well known that even in the absence of Mn, the Si(001) surface can form numerous defect structures. However, defects cannot account for the unique rowlike structures observed in the STM images. On the clean Si(001) surface, defects have been studied extensively, and their appearance in STM images is well understood.[14–17] Most frequently, missing dimer defects have been observed, which are also largely accountable for the black regions (holes) in Fig. 1(c). Missing dimer defects can also be present on a clean, well-ordered Si(001) surface, but with much lower probability.

Likewise, pure Si adatom islands on Si(001) have been reported to form rowlike structures in the early stages of homoepitaxy.[18] However, the monolayer height of these islands is typically 1.3 Å, different from the 1.1 Å height of the rowlike structures observed in the STM images in Fig. 1 and the height cross section displayed in Fig. 5. Moreover, the bright protrusions in Figs. 1(b)–1(f) could not be observed on clean Si(001) surfaces without depositing Mn. In addition, the $c(4\times2)$ reconstruction of clean Si(001) would give rise to STM images which significantly differ on the atomic scale from the Mn-induced structure with the same local periodicity.

Hence, we conclude that the bright row structures that are being formed perpendicular to the rows of the underlying surface are due to incorporated Mn atoms into the next layer of Si. Three arguments can be given to confirm that these Mn atoms occupy subsurface interstitial sites. First, the subsurface interstitial site is calculated to be the most stable site, lower in energy than any on-surface or bulk interstitial site.[7,10,19] Second, in all other periodic structures we considered, the Mn-induced electronic states give rise to an appearance of the simulated STM images different from those for subsurface incorporation [compare Figs. 2(b)–2(d)]. In particular, the acquired STM images are incompatible with the hypothesis of rows of substitutional Mn atoms [Fig. 2(c)]. Third, there is quantitative agreement (as discussed below) between the corrugation in the experimentally obtained STM images and in the row structures simulated for subsurface interstitial sites as displayed in Fig. 5.

The DFT calculations tell us that the stability of Mn in the subsurface interstitial site is related to its high coordination. In order to achieve this, the Mn atom establishes chemical bonds to the neighboring Si atoms on the expense of the Si-Si surface bond that is considerably weakened, indicated by an increase of 0.4 Å of the Si-Si dimer bond length compared to the clean Si(001) surface. At the same time, the surface Si atoms above the Mn move outward from the surface.

Interestingly, the DFT calculations show that the physical position of the Si dimers with Mn underneath are topographically *higher*. However, this height difference is not fully reflected in both the calculated and measured STM images. When the Mn atom is present, electrons are pulled into the newly formed Mn-Si bonds below the surface, making the surface Si atoms, in the presence of Mn, appear less bright. Comparison of the absolute height scales for the two DFT images in Figs. 2(a) and 2(b) reveals that Fig. 2(b) is overall 0.2 Å lower than the image of the clean surface, Fig. 2(a). This occurs despite the fact that the positions of the Si atoms with the Mn below are higher than normal for a clean Si dimer.

This electronic effect overcompensates the geometric effect in both the computed as well as the measured images. The Si dimers *without* Mn below them adjacent to those *with* Mn below them appear even darker, as evidenced by the grayish parts between the bright spots of Fig. 2(b). This is attributed to the electrons in the dangling bonds of these Si dimers moving into the Mn-Si bonds at the other, neighboring dimer. This electronic effect explains why the middle Si dimer with incorporated Mn does not appear 1.3 Å above the terrace, but only about 1.1 Å [cf. Fig. 1(g)]. This effect is also responsible for the height difference of 0.6 Å between the Si dimers with Mn below and without Mn below in the

same terrace as displayed in Fig. 5. As explained above, these "normal" Si dimers appear to be lower than expected (although geometrically, they are at their usual height) due to electronic effects, since part of their charge has been pulled away into the Mn-Si bonds in the neighboring dimer.

Our results are in qualitative agreement with calculated STM images of isolated Mn atoms on Si(001).[19] Moreover, our calculations show that the subsurface Mn atoms widen the Si lattice around the interstitial site. As a consequence of these distortions, two Mn atoms in the same Si dimer row interact repulsively. For adjacent interstitial sites, the interaction energy is 0.4 eV/Mn. Therefore, only half of the available sites are occupied by Mn, giving rise to a local Mn coverage of a quarter of a monolayer with either a (2×2) or $c(4\times2)$ local arrangement of the Mn atoms. While the formation energy of these two structures is the same within the accuracy of our calculations, only the $c(4\times2)$ arrangement has been observed in the experiment when two rows were observed next to each other.

VI. CONCLUSION

Under suitable preparation conditions, two-dimensional rowlike structures could be created by the deposition of 0.1 ML Mn on Si(001) and subsequent annealing, besides the three-dimensional Mn-silicide islands reported previously. By combining STM images with first-principles calculations, we could identify these rowlike structures as being due to Mn atoms in subsurface interstitial sites arranged in a local $c(4\times2)$ pattern. No evidence for substitutional incorporation of Mn was found. This makes it unlikely that similar physical concepts could be used to turn Si into a diluted magnetic semiconductor as has been demonstrated for Mn-doped Ge.[3,4] Yet, the observed two-dimensional structures induced by Mn could be useful for achieving δ-layer doping of Si by Mn. Likewise, the observed interstitial incorporation of Mn is compatible with the atomic structures associated with the predicted ferromagnetism of flat Mn-Si islands or films on Si(001).[7]

ACKNOWLEDGMENTS

This work was supported by the National Science Foundation CAREER-DMR-0349108, New York State Office of Science, Technology and Academic Research Faculty Development Program (NYSTAR-FDP-C020095), and MARCO Interconnect Focus Center. The work at Fritz-Haber-Institut was in part supported by Deutsche Forschungsgemeinschaft within Research Center SFB290. M.H., P.K., and M.S. would like to thank Paul Fumagalli, Jens Paggel, and Holger Lippitz (FU Berlin) for discussions about their unpublished results.

*Electronic address: vlabella@albany.edu
†Present address: Fachbereich Physik, Universität Duisburg-Essen, 47048 Duisburg, Germany.

[1] A. J. R. da Silva, A. Fazzio, and A. Antonelli, Phys. Rev. B **70**, 193205 (2004).
[2] M. Bolduc, C. Awo-Affouda, A. Stollenwerk, M. B. Huang, F. G. Ramos, G. Agnello, and V. P. LaBella, Phys. Rev. B **71**, 033302 (2005).
[3] S. Cho, S. Choi, S. C. Hong, Y. Kim, J. B. Ketterson, B.-J. Kim, Y. C. Kim, and J.-H. Jung, Phys. Rev. B **66**, 033303 (2002).
[4] Y. D. Park, A. T. Hanbicki, S. C. Erwin, C. S. Hellberg, J. M. Sullivan, J. E. Mattson, T. F. Ambrose, A. Wilson, G. Spanos, and B. T. Jonker, Science **295**, 651 (2002).
[5] H. Wu, P. Kratzer, and M. Scheffler, Phys. Rev. Lett. **98**, 117202 (2007).
[6] D. J. Monsma, R. Vlutters, and J. C. Lodder, Science **281**, 407 (1998).
[7] H. Wu, M. Hortamani, P. Kratzer, and M. Scheffler, Phys. Rev. Lett. **92**, 237202 (2004).
[8] M. R. Krause, A. Stollenwerk, M. Licurse, and V. P. LaBella, J. Vac. Sci. Technol. A **24**, 1480 (2006).
[9] H. Lippitz, J. J. Paggel, and P. Fumagalli, Surf. Sci. **575**, 307 (2005).
[10] M. Hortamani, H. Wu, P. Kratzer, and M. Scheffler, Phys. Rev. B **74**, 205305 (2006).
[11] M. Krause, A. Stollenwerk, C. Awo-Affouda, B. Maclean, and V. P. LaBella, J. Vac. Sci. Technol. B **23**, 1684 (2005).
[12] P. Blaha, K. Schwarz, G. K. H. Madsen, D. Kvasnicka, and J. Luitz, WIEN2K, an augmented plane wave+local orbitals program for calculating crystal properties, Technische Universität, Wien, Austria, 2001.
[13] J. Tersoff and D. R. Hamann, Phys. Rev. B **31**, 805 (1985).
[14] D. Riedel, M. Lastapis, M. G. Martin, and G. Dujardin, Phys. Rev. B **69**, 121301(R) (2004).
[15] R. M. Tromp, R. J. Hamers, and J. E. Demuth, Phys. Rev. Lett. **55**, 1303 (1985).
[16] R. J. Hamers and U. K. Köhler, J. Vac. Sci. Technol. A **7**, 2854 (1989).
[17] S. R. Schofield, N. J. Curson, J. L. O'Brien, M. Y. Simmons, R. G. Clark, N. A. Marks, H. F. Wilson, G. W. Brown, and M. E. Hawley, Phys. Rev. B **69**, 085312 (2004).
[18] Z. Zhang and M. G. Lagally, Science **276**, 377 (1997).
[19] G. M. Dalpian, A. J. R. da Silva, and A. Fazzio, Phys. Rev. B **68**, 113310 (2003).